Regular Article

HEMATOPOIESIS AND STEM CELLS

Multimodal imaging reveals structural and functional heterogeneity in different bone marrow compartments: functional implications on hematopoietic stem cells

Francois Lassailly,[1,2] Katie Foster,[1] Lourdes Lopez-Onieva,[1] Erin Currie,[1] and Dominique Bonnet[1]

[1]Haematopoietic Stem Cell Laboratory and [2]In Vivo Imaging, London Research Institute, Cancer Research UK, London, United Kingdom

---

Key Points

- Comparative analysis of epiphyses, diaphyses, and calvaria in terms of homeostatic HSC content, homing, and early reconstitution is described.
- Noninvasive intravital imaging of intact bones and assessment of BVF, BRA, and hypoxia are reported.

Intravital microscopy of the calvarium is the only noninvasive method for high-resolution imaging of the bone marrow (BM) and hematopoietic stem cell (HSC) niches. However, it is unclear if the calvarium is representative of all BM compartments. Using the combination of whole body optical imaging, intravital microscopy, and "in vivo fluorescence trapping," a thorough comparison of HSCs and putative HSC niches in the calvaria, epiphyses, and diaphyses, at steady state or after HSC transplantation, can be made. We report substantial heterogeneity between different BM compartments in terms of bone-remodeling activity (BRA), blood volume fraction (BVF), and hypoxia. Although BVF is high in all BM compartments, including areas adjacent to the endosteum, we found that compartments displaying the highest BVF and BRA were preferentially seeded and engrafted upon HSC transplantation. Unexpectedly, the macroanatomical distribution of HSCs at steady state is homogeneous across these 3 areas and independent of these 2 parameters and suggests the existence of "reconstituting niches," which are distinct from "homeostatic niches." Both types of niches were observed in the calvarium, indicating that endochondral ossification, the process needed for the formation of HSC niches during embryogenesis, is dispensable for the formation of HSC niches during adulthood. (*Blood*. 2013;122(10):1730-1740)

Introduction

Despite a tremendous increase in our understanding of hematopoietic stem cell (HSC) niches during the past 2 decades, the precise localization, composition, and regulation of these niches remain highly controversial.[1] A number of different components have been shown to be integral to their constitution, including cells (osteoblasts, endothelial cells, mesenchymal stem cells, CXCL12-abundant reticular cells, osteomacs, osteoclasts, regulatory T cells, and nonmyelinated Schwann cells), as well as various bound and soluble growth factor chemokines, extracellular matrix components, ions, and gases.[2-5] Two distinct types of HSC niches have been reported: the osteoblastic niche, located in the endosteal region (within 12 cell diameters[6] [~100 μm] from the bone surface), and the vascular niche, remote from the endosteum and in close proximity to blood vessels. The epiphyses, the extremities of the long bones, contain trabecular bone and are thought to be enriched for osteoblastic niches as compared with the diaphysis,[7] the shaft of the long bones, which is composed of cortical bone. Previously, the endosteal region was believed to be poorly vascularized, especially in the epiphyses,[3,8-10] supporting the concept that osteoblastic niches were distinct from the vascular niche and hypoxic.[11,12]

To better characterize and understand the biology of HSC niches, different imaging modalities have been developed to visualize single HSCs within live bone marrow (BM).[13-17] Each imaging approach has particular features with respect to the BM compartment that can be analyzed.[17] The work of Dr Mazo in Prof von Andrian's group pioneered the technique of noninvasive intravital microscopy of the BM. They have shown that the calvarium, the frontoparietal bone of the skull, is a unique site where the thin bone is compatible with direct observation and time-lapse recording of single cells without damaging the tissues.[18] This strategy has now been exploited in a variety of applications for analyzing the homing and lodgment of various cell types to the BM,[4,15,18-23] studying thrombopoiesis,[24] and dissecting BM immunologic functions.[25-27] However, the extent to which these observations are universal and apply to other BM compartments has yet to be shown.

The BM is generally regarded as a homogeneous organ, spread throughout different bones wherein a BM sampling from a given site is thought to be representative of the whole organ status. However, it is well known that with aging, red BM, which is hematopoietically active, shifts toward yellow marrow, which is mostly filled with adipocytes and is hematopoietically inactive.[28] This shift starts from the distal extremities of the long bones and the tail in mice, resulting in very different composition of BM in different areas of the skeleton with age. With respect to bone, their structures, development, and biological characteristics are heterogeneous: the epiphyses/metaphyses contain trabecular bone as well as the growth plate, whereas the diaphyses do not. The former are more dynamic in terms of bone remodeling than the diaphyses, and reports have indicated epiphyses

---

are enriched in HSC niches.[7] In contrast, the calvarium is a flat bone, devoid of trabeculae, presenting various singularities in terms of bone composition[29] and remodeling processes,[30-32] which might impact the microenvironment within.[33] Importantly, it has been shown that during development in the mouse, the endochondral ossification process involved in the growth of long bones is necessary for the formation of HSC niches.[34] In contrast, the calvarium develops through intra-membranous ossification, which raises the question of the very presence of HSC niches in this bone. It has been shown that the BM of the skull contains hematopoietic progenitor cells[18,35] and is frequently a site for initiation of murine and human hematopoietic reconstitution.[36,37] However, the presence of functional long-term HSCs, and thus HSC niches, has not yet been demonstrated in the calvarium.

Here, with the aim of characterizing the BM of the calvarium, we have developed and adapted contrasting and imaging procedures to assess its structure and the functionality of cells within, as compared with the epiphyses/metaphyses and diaphyses. We provide evidence that BM compartments are heterogeneous, both structurally and functionally, which impacts hematopoietic reconstitution following irradiation and transplantation, but not the steady-state localization of HSCs.

Materials and methods

Mice

Wild-type C57BL6 (CD45.2) mice were purchased from Charles Rivers, and congenic C57Bl6 CD45.1 were bred at the institute. They were enrolled between 7 and 12 weeks. Reporter β-actin-luciferase mice were purchased from CaliperLifeSciences. All animal experiments were performed in accordance with Home Office and Cancer Research UK guidelines.

Collection of BM cells from diaphyses, epiphyses, and calvaria

Epiphyses were dissected from the diaphysis by cutting the extremities of the cortical bone (shaft) (see annotated micro–computed tomography [CT] model in supplemental Figure 3A; see the *Blood* Web site). Epiphyses, diaphyses, and calvaria were crushed separately in phosphate-buffered saline (PBS) 2% heat-inactivated fetal calf serum supplemented with heparin and 0.1 mg/mL DNase I.

Probes and reagents for in vivo contrasting procedures

Fluorescent pamidronate (Osteosense) and fluorescent blood pool agent (Angiosense) were purchased from Visen Medical. IsolectinB4 (IB4)–AlexaFluor conjugates, nontargeted Quantum dots655, and Hoechst33342 (HO) were obtained from Invitrogen. Pimonidazole (PIM; Hypoxyprobe) was purchased from Natural Pharmacia International, Inc.

Imaging systems

The near-infrared scanner Odyssey (LiCor) was used as previously described for ex vivo imaging of dissected organs.[38] Bioluminescence imaging (BLI) was performed using the IVIS Spectrum (Caliper Life Sciences).

Confocal/multiphoton microscopes, namely, an inverted LSM510 (Zeiss) and an upright LSM710NLO (Zeiss) equipped with a MaiTai "High Performance" fully automated 1-box mode-locked Ti:Sapphire laser with DeepSee dispersion compensation (Spectra-Physics) and a 633-nm laser for multiphoton and confocal capability, respectively, were used in this study.

Image processing, reconstruction, analysis, and display were performed using Imaris 6.3 and 7.4 (Bitplane).

Imaging of live BM in the calvarium

After appropriate incubation upon administration of the desired contrasting agents, mice were euthanized by cervical dislocation, the skin was removed, and the intact skull was immersed in PBS for direct examination of the calvarium under the microscope.

Long bones

Most of the analyses were performed by direct sectioning of fresh un-processed bones using a razor blade. Alternatively, bones were embedded in optimum cutting temperature compound and snap frozen at −80°C before sectioning.

Ratiometric three-dimensional (3D) quantification of blood vessel density (BVD)

IB4-contrasted femurs and tibias were dissected, cut fresh or after snap freezing using a scalpel. IB4, second harmonic generation (SHG), and reflectance were collected simultaneously. Image processing was performed using Imaris6.3 (Bitplane) software as follows: for each acquisition, a 3D region of interest was drawn in the endosteal region (as defined by maximum 90 μm from the bone toward central BM) and in the central part of the BM (>100 μm from the bone). The volume and total IB4-associated fluorescence intensities were extracted and used to calculate the blood volume fraction (BVF = fluorescence intensity/volume). For each pair (endosteal/central BM), the ratio of BVF endosteal/BVF central BM was calculated.

In vivo quantification of perfusion efficiency

HO perfusion was done following published procedures.[11,12] After cervical dislocation, femurs, calvaria, spleen, and thymus from C57Bl6 or β-actin-luciferase mice were quickly dissected and immediately immersed in ice-cold PBS and kept on ice. All steps were carried out on wet ice. After crushing, erythrocytes were lysed with ammonium chloride, and cells were stained with monoclonal antibodies for analyzing hematopoietic stem and progenitor cell (HSPC) markers. Specific HO uptake was calculated by dividing the geometric mean fluorescence intensity of the HO blue channel by the same analysis carried out on the same population of cells from the same organ but from an animal not injected with HO (negative control). This corresponds to the specific fluorescence intensity and reflects the actual uptake of HO by the population of interest.

Detection of PIM adducts

Wild-type mice were injected with 125 mg/kg PIM or saline solution and euthanized after 2 hours (different time points were previously tested). BM, spleen, and thymus were rapidly harvested and kept in PBS at 4°C. Cells were recovered and processed following previously reported procedures. Cells from PIM noninjected animals but stained with the same concentration of relevant antibody after permeabilization were used as a negative control to calculate the specific geometric mean fluorescence intensity as previously reported.[38]

Noninvasive quantitative in vivo BLI

Non–stem cells (lineage low; Sca-1⁻; S⁻), progenitors (lineage negative; Lin⁻), or enriched stem cells (Lin⁻Sca-1⁺c-kit⁺; LSK) were sorted from β-actin-luciferase lineage–depleted BM cells recovered from calvaria, epiphyses, or diaphyses. Cells were intravenously injected in the tail of nonirradiated or sublethally irradiated (375 cGy) 8- to 12-week-old NOD/SCID mice. BLI acquisitions were performed as previously described[39] after intraperitoneal injection of luciferin (125 mg/kg; Caliper Life Science) and imaging on dorsal and ventral sides.

In vivo fluorescence trapping

After injection of the designated near-infrared (NIR) probe (blood pool agent or pamidronate) and appropriate incubation (10-15 minutes and 24 hours, respectively), calvarium, femur, tibia, and spleen were dissected and immersed in PBS at 4°C. For each animal, the calvarium, a pool of 6 epiphyses, a pool of 4 diaphyses, and the spleen were analyzed separately as follows: bones were crushed in PBS + 2% fetal calf serum and placed in a well of a 24-well plate. Fluorescence intensity was measured using the Odyssey infrared imaging

system (Ly-Cor Biosciences). After fluorescence acquisition, each well was thoroughly mixed and an aliquot was used to count the number of cells. Standardized quantification of fluorescence-integrated intensity was determined using the Odyssey MousePOD module (version 2.1.12). Identical procedures were implemented with a noninjected animal. Within each experiment, all data were normalized by the negative control before being divided by the number of cells in the compartment ($=$ BVF/10^6 cells or bone-remodeling activity [BRA]/10^6 cells). For each animal, the results were expressed as a percentage of the diaphysis compartment.

Reverse transcription and real-time polymerase chain reaction (PCR)

Dissected bone compartments were crushed at $+4°C$ with precooled guanidium thiocyanate-based extraction buffer, and total RNA was isolated with the RNeasy Mini Kit (Quiagen). Messenger RNAs (mRNAs) were reverse transcribed by Superscript III Reverse Transcriptase (Invitrogen) with an oligo dT primer (Sigma-Aldrich). Real-time PCR was performed with an ABI Prism7900H Thermal Cycler (Applied Biosystems) using SYBR Green dye. RNA was quantified with the comparative CT method with β-actin (Actb) as a housekeeping gene. Primers used were the following: Actb (Mm_Actb_2_SG, QuantiTec Primer Assay); osteocalcin sense, TTCTGCTCACTCTGCTG ACCCT; antisense, CCCTCCTGCTTGGACATGAA; cathepsin K sense, GGCTGTGGAGGCGGCTAT; antisense, AGAGTCAATGCCTCCGTTC TG; vascular endothelial (VE)-cadherin sense, CCATCTTCCTCTGCATC CTC; antisense, CAACTGCTCGTGAATCTCCA; vascular endothelial growth factor receptor 2 (VEGFR2) sense, TTTGGCAAATACAACCCTTCAGA; and antisense GCAGAAGATACTGTCACCACC.

BM transplantation and early reconstitution

Unless otherwise stated, CD45.2 C57Bl6 mice were lethally irradiated (2×500 Gy with 4 hours apart) 24 hours before to receive a BM transplant from CD45.1 congenic donors by tail vein injection. Chimerism level was assessed using anti–CD45.1-allophycocyanin and CD45.2-fluorescein isothiocyanate (FITC) antibodies and calculated as follows: donor-derived chimerism $=$ number CD45.1$^+$ cells/number (CD45.1$^+$ $+$ CD45.2$^+$) live cells $\times$ 100. As many events as possible were acquired for each sample, typically between 2×10^6 and 5×10^6.

Homing experiments

Twenty-four hours after lethal irradiation, CD45.2 recipients received intravenous infusion of 17×10^6 to 37×10^6 BM-mononuclear cells from CD45.1 congenic donors. Sixteen hours later, bones were analyzed by flow cytometry. A negative control (noninjected) was used to objectively discriminate between autofluorescence and CD45.1-positive cells. As many events as possible were acquired for each sample, typically between 3×10^6 and 7×10^6.

Statistical analyses

Microsoft Excel 2004 for Mac (version11.5.5) was used to evaluate the significance. Student t tests (paired when appropriate) were used. P values $< .05$ were considered significant.

Results

### BVD is very high in every BM compartment, including in close proximity to the bone surface

We first aimed to characterize the macro-anatomical structure of the calvarium as compared with the long bones in terms of BM cavities and BVD. We contrasted the endosteum of the calvarium using an NIR-conjugated fluorescent pamidronate (NIR-pamidronate). This probe accumulated within known places of dynamic BRA (the metabolic process allowing bone renewal and growth), confirming the efficiency and specificity of this marker (supplemental Figure 1).[40] At

higher magnification, NIR-pamidronate imaging within the calvarium reveals that the BM is contained within a complex network of small diameter, interconnected cavities (Figure 1A-B). The biggest cavities can also be visualized by micro-CT (supplemental Figure 2A), and together this demonstrates that the BM content in this bone is limited (supplemental Figure 4). To visualize the vascularization of the calvarium, we initially used nontargeted Quantum dots as a blood pool agent and 3D multiphoton acquisition (Figure 1C; supplemental Figure 2B; supplemental Movie 1). Using this approach, the endosteal region and vasculature of the calvarium can be visualized simultaneously. However, because the use of nontargeted blood pool agents is compromised when vascular integrity is altered (eg, after irradiation or after bone sectioning), we circumvented this limitation by contrasting the endothelial cells of the blood vessels instead of the circulating plasma. Intravenous perfusion with fluorescently conjugated IB4 enabled us to contrast the BM endothelium of live animals, allowing subsequent examination of BM endothelium by intravital microscopy (supplemental Figure 2C-D).

Using the previous in vivo contrasting procedures, we observed a very high BVD in the BM of the calvarium, including the areas adjacent to the bone (Figure 1D-F). To determine whether this was a specific feature of flat bones, we applied similar procedures to long bones, which the conventional blood pool agents would not allow. Although the structure of the vasculature was different from what we observed in the calvaria, long bones also displayed a very high BVD, throughout the central cavity and the endosteum, in the diaphysis, epiphysis, and metaphysis (Figure 1G-J). As the endosteal region and osteoblastic niche have previously been reported to be poorly vascularized,[3,8-10] we quantified and compared the BVD within the endosteal region and the central BM. Using a volumetric measurement in different regions on the same 3D data set, we found that BVD in the endosteum is not lower than in the central part of the BM (BVD endosteum/BVD central BM $= 1.2 \pm 0.37$; n $= 6$, from 3 animals). These structural observations indicate that osteoblastic and vascular niches are not mutually exclusive. Instead, the proximity of the blood vessels/sinusoids to the bone surface suggests they might well be components of the osteoblastic niche, more accurately being described as an osteovascular niche, at least at a structural level.

BM has high perfusion efficiency, but most primitive HSCs are hypoxic

Previous reports have described the HSC niche as hypoxic due to poor perfusion.[11,12,41] Given the high BVD we observed throughout the BM, we were interested in the existence of hypoxic areas despite being vascularized. To survey how functional these vascular networks are, we performed a conventional perfusion assay based on intravenous injection of HO.[11,12] Perfusion efficiency was determined in the diaphyses, epiphyses, and calvaria (supplemental Figure 3A). The thymus was used as a positive control for hypoxia,[42] and the spleen as a control for high perfusion efficiency. Strikingly, although 14% of splenocytes were HO negative, $<2\%$ of the cells from the diaphysis, epiphysis, and calvarium were negative (Figure 2A). No difference in perfusion efficiency could be evidenced between diaphyses, epiphyses, or calvaria. Despite the high perfusion efficiency of all 3 BM compartments, as reported previously, the more primitive HSCs (CD45$^+$Lin$^-$Sca-1$^+$c-kit$^+$CD150$^+$; LSK-CD150) and HSPCs (CD45$^+$Lin$^-$Sca-1$^+$c-kit$^+$; LSK) were less efficiently perfused as compared with their more mature counterparts (Figure 2C,E). We confirmed this observation by quantifying the amount of truly hypoxic cells using PIM staining, a marker of hypoxia that forms covalent adducts with proteins in cells exposed
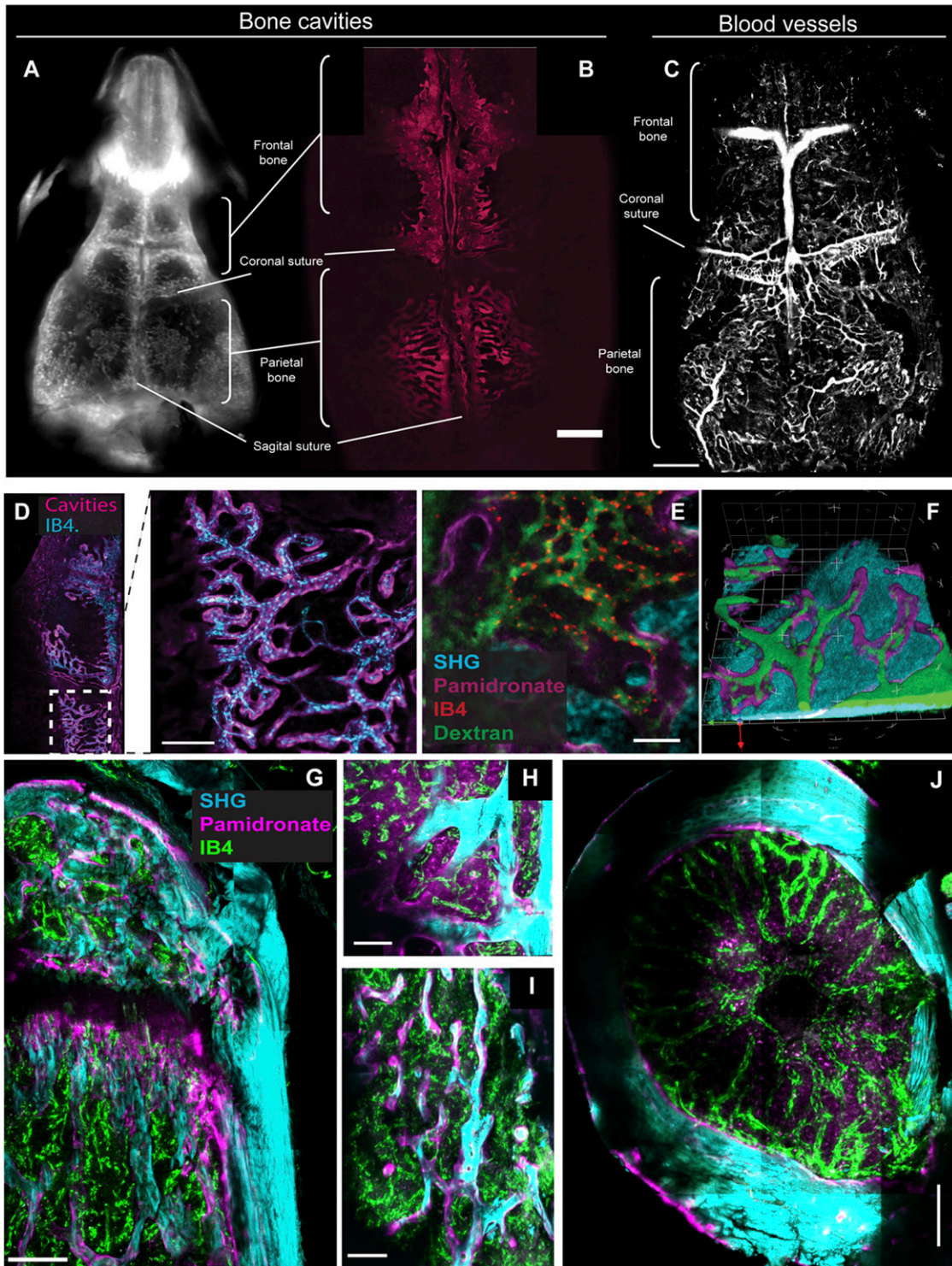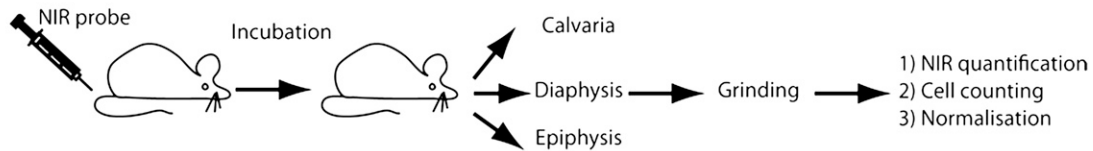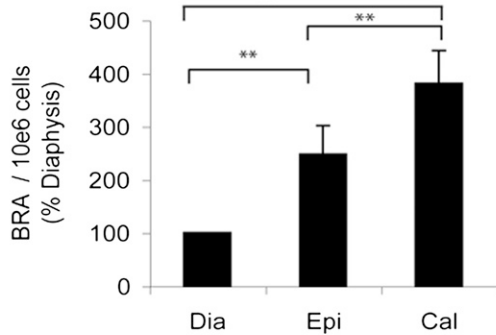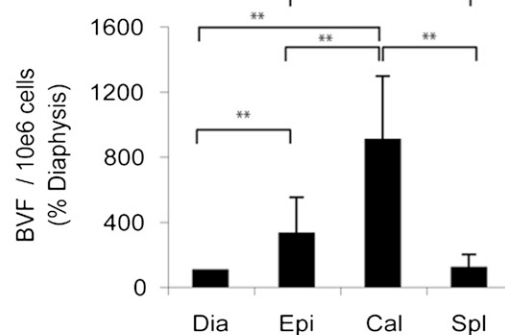
Figure 1. Comparison of the vascularization in calvaria and long bones. Structural characterization of the calvarium using in situ imaging of BRA as revealed by an NIR-pamidronate probe. Visualization using an NIR scanner (A) and confocal microscope (B). Scale bar represents 700 μM. (C) A 3D reconstruction of BM vasculature in the calvarium where blood vessels are contrasted using nontargeted Quantum dots. The 3D tiling was applied to acquire 16 × 23 adjacent stacks of 15 steps, covering a 6800-μm/9780-μm/600-μm volume. Scale bar represents 1 mm. (D) Combined BRA and vasculature contrasting obtained after intravenous injection of NIR-pamidronate and IB4-Alexa568, imaged in intact BM. Vasculature can be seen to be in close contact with the bone. Scale bar represents 300 μm. (E) Four-color live tissue imaging combining NIR-pamidronate (endosteum), IB4-Alexa568 (endothelial cells), and FITC-dextran (blood plasma) with simultaneous detection of SHG (bone). (F) A 3D model of bone (SHG, blue), bone endosteum (NIR-pamidronate, purple), and blood vessels contrasted with FITC-dextran (green). (G-J) Ex vivo imaging of long bones (SHG, cyan) after in vivo contrasting with NIR-pamidronate (purple) and IB4-Alexa488 (green). Sagittal section of tibia epiphysis (G) with details of the trabecular region (H). Scale bars represent 200 and 100 μm, respectively. Transverse section of femur metaphysis (I) and diaphysis (J). Scale bar represents 200 μm.
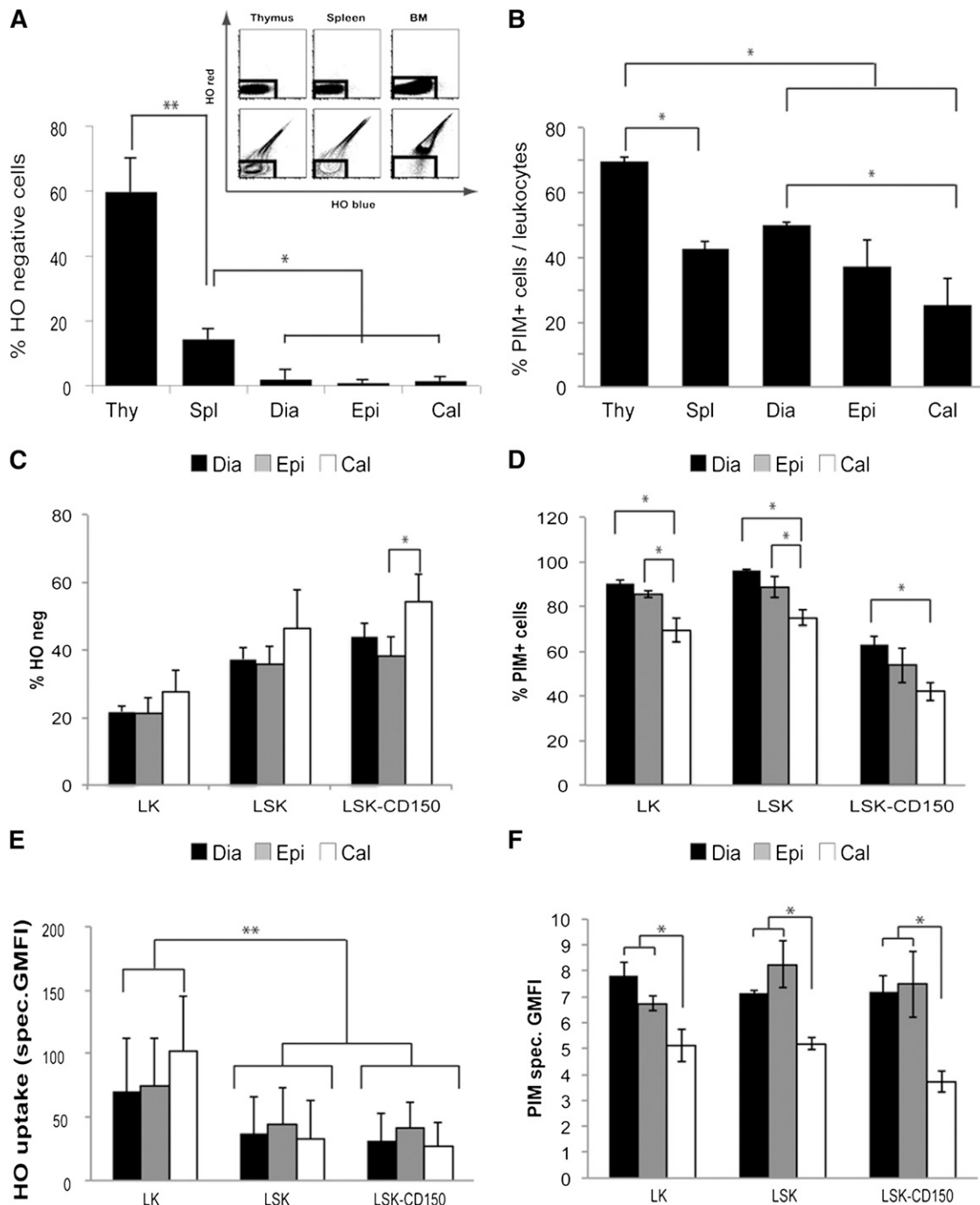
Figure 2. Analysis of the hypoxic status of BM and HSCs. (A) In vivo HO perfusion efficiency analyzed simultaneously in the thymus, spleen, and BM. Negative cells were defined using a noninjected control, based on both HO blue and HO red fluorescence (see inset: fluorescence-activated cell sorter [FACS] analysis; upper panel, control; lower panel, HO injected). The gates indicated in the FACS panels (inset) were used to analyze the percentage of HO-negative cells from animals infused with HO, 5 and 10 minutes before being euthanized. Average values are displayed ± standard deviation (SD) (n = 3). *P < .05; **P < .005. (B) Frequency of PIM-positive leukocytes within the designated compartments. Average ± SD is displayed (n = 3). Percentage (±SD) of HO-negative cells (C) and PIM+ cells (D) within the LK, LSK, and LSK-CD150 cells from Dia, Epi, and Cal (n = 3 and 3, respectively). Specific HO (E) and PIM (F) uptake within HSPCs from Dia, Epi, and Cal (n = 7 from 2 independent experiments and n = 3, respectively). *P < .05 or **P < .005. Cal, calvaria; Dia, diaphyses; Epi, epiphyses.

to low oxygen pressure (<10 mm Hg). This confirmed the presence of hypoxic cells both in the spleen and the BM (Figure 2B). It also revealed that, despite similar perfusion efficiency of all 3 BM compartments (Figure 2A,C,E), the frequency of hypoxic cells within the calvarium tends to be reduced as compared with the epiphysis and diaphysis (Figure 2B). This was also verified for HSPC subpopulations, by analyzing the frequency of PIM+ cells as

well as the intensity of PIM uptake (Figure 2D,F). Surprisingly, most lineage–c-kit+ (LK) and LSK cells were PIM+, and only 40% to 60% of LSK-CD150 displayed PIM reactivity (Figure 2D). We further analyzed the phenotype of hypoxic cells and found that <1% of HO-negative or PIM-positive BM cells displayed an LSK or LSK-CD150 phenotype, confirming that hypoxia is not a specific feature of stem cells (supplemental Figure 3B-D).
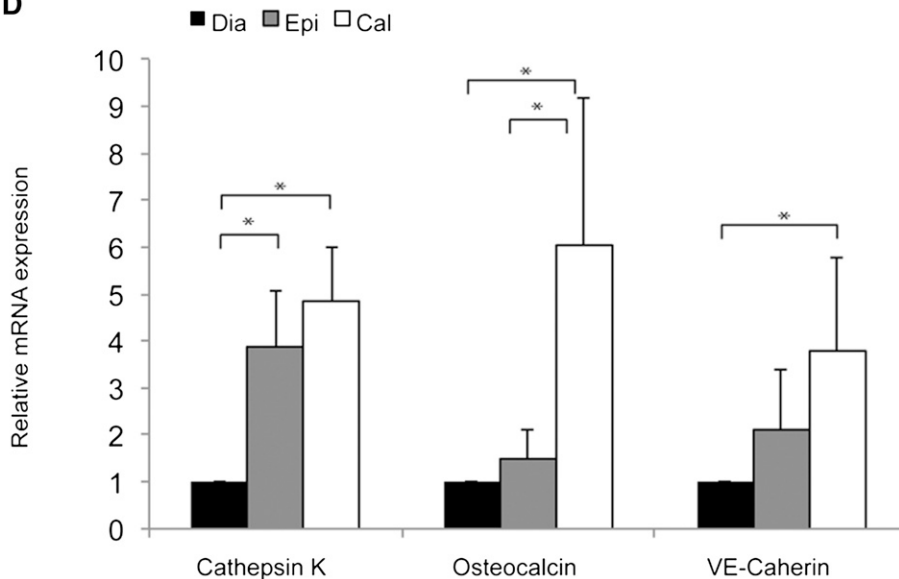
Figure 3. Quantification of putative stem cell niche markers in different steady-state BM compartments. (A) Diagram displaying the process of in vivo fluorescence trapping. For each sample, total fluorescence intensity and number of cells were measured ex vivo to calculate the fluorescence intensity per 10^6 cells. (B) Quantification of BRA using NIR-pamidronate in vivo fluorescence trapping. Average values from 4 animals $\pm$ SD are displayed (n = 2 experiments). (C) Quantification of BVF using NIR blood pool agent in vivo fluorescence trapping in identical conditions as previously, except a 10- to 15-minute incubation after in vivo administration. Data are average values from 6 animals (3 experiments) $\pm$ SD. *$P < .05$ or **$P < .005$. (D) Quantitative reverse-transcription–PCR quantification of osteoclast (cathepsin K), osteoblast (osteocalcin), and endothelial cell (VE-cadherin and VEGFR2) specific mRNAs. CT values used were the result of 2 different duplicates from 4 independent experiments.

From this, it appears that although the BM is highly vascularized, most HSPCs are located in areas of the BM that are poorly perfused and display evidence of hypoxia, irrespective of the compartment in which they reside. It is worth noting that the hypoxic status of calvaria HSPCs might be less pronounced as compared with their long bone counterparts.

BM compartments are heterogeneous for BRA and BVF

Most of the current knowledge on HSC niche localization relies on the assumption that HSCs are in their niche and therefore adjacent cells are niche components.[5,7,14,15,43-46] Previous reports have suggested that some regions of the skeleton, such as the trabecular region of the long bones, might be enriched in stem cell niches.[3,7] From these assumptions, we wondered if BRA, indicative of osteoclast/osteoblast activity, could be informative of the osteoblastic niche[33] and whether BVF, which quantifies the vasculature, could provide information on the vascular niche.

As it was not appropriate to perform quantifications based on the microscopy techniques used previously (Figure 1), we developed a new strategy that we call "in vivo fluorescence trapping." This method of quantification is based on the in vivo infusion of fluorescent probes, where the concentration of the probe per million cells can be measured in tissues after dissection (Figure 3A). We used NIR probes to ensure maximum sensitivity and reliability.[47] The BRA was quantified after NIR-pamidronate contrasting (Figure 1;

supplemental Figure 1). We found that BRA is 2.5-fold higher in epiphyses as compared with diaphyses, which provided a good validation of the assay (Figure 3B). In the calvarium, activity is 3.8 times higher than in the diaphysis (Figure 3B), indicating an even higher level of BRA.

In order to compare the proportion of blood vessels in the different compartments, we also used this approach to measure the relative amount of blood vessels. The use of an NIR blood pool agent was used to quantify the amount of plasma circulating in the blood vessels of each compartment, a parameter defined as BVF. It revealed that BVF in the epiphysis and calvarium is 3.2 and 9 times higher, respectively, as compared with the diaphysis (Figure 3C). Interestingly, BVF was equivalent in the spleen and diaphysis.

In vivo fluorescence trapping results were further corroborated by quantitative reverse-transcription PCR. As expected, osteoclast- and osteoblast-specific transcripts (cathepsin K and osteocalcin, respectively) were more abundant in the regions displaying high BRA, whereas VE-cadherin, an endothelial-specific transcript, was more abundant in regions showing high BVF (Figure 3D). By contrast, VEGFR2 transcripts that are expressed by endothelial and hematopoietic subsets displayed homogeneous expression in the 3 compartments (data not shown).

Discrepancies between the 2 quantification methods are not surprising, because mRNA abundance for these transcripts only provides an estimation of the frequency of cell types, which might not be directly proportional to the activity of these cells or the volume of blood within the same compartment.

Homeostatic stem cells are homogenously distributed throughout diaphyses, epiphyses, and calvaria, independently of BVF or BRA

Having observed differences in hypoxia, BVF, and BRA between the diaphysis, epiphysis, and calvarium, we were next interested in determining whether this correlated with the frequency of HSC niches in each compartment, and therefore the number of HSCs. We were also interested in determining whether the calvarium contains niches similar to the long bones given the differences in these parameters. To test this, we analyzed the frequency of different HSPC populations in the 3 BM compartments. Contrary to our expectations, we were unable to demonstrate any difference in the frequency of the different HSPC subpopulations between the diaphysis, epiphysis, and calvarium, even in the most primitive LSK-CD150+ cells (Figure 4A), despite differences in respective cell numbers (supplemental Figure 4).

Having observed no difference in frequency of HSCs between the compartments despite the heterogeneity found in BRA, BVF, and hypoxia, we next tested whether there was an effect on HSC function using engraftment assays. Using noninvasive BLI, we were able to follow the early stages of hematopoietic reconstitution after intravenous injection of small numbers of LSK cells (1250 cells per recipient). Seven days postinfusion, no qualitative difference was noted in the distribution of the graft, irrespective of the origin of the HSPCs (Figure 4B). We quantified the dynamics of hematopoietic reconstitution using bioluminescence and observed a similar increase in signal intensity from all 3 HSPC sources (Figure 4C). The primitive LSK-CD150 cells derived from the 3 BM compartments displayed similar HO uptake irrespective of their origin (Figure 2E), suggesting they should have similar long-term HSC (LT-HSC) engraftment ability.[12] To confirm this observation, we performed long-term repopulating assays using HSPCs from the calvarium or the legs to reconstitute lethally irradiated congenic recipients. Thirteen weeks posttransplantation, the multilineage chimerism was similar in both

groups (Figure 4D). Competitive secondary transplantations were performed using BM from the legs of reconstituted recipients for an additional 19 weeks (32 weeks in total). Again, no functional difference was observed between the 2 sources of the primary graft (Figure 4E). Altogether, these results indicate that homeostatic LT-HSCs, and by extension HSC niches, are, at least macroscopically, evenly distributed across the skeleton despite heterogeneous levels of BRA, BVF, and hypoxia.

HSCs preferentially home and engraft BM compartments displaying high BRA and BVF, suggesting the existence of "reconstituting niches"

It was unexpected to find an even distribution of HSCs across the different BM compartments at homeostasis, and we next investigated whether there were any differences during the reconstitution process after HSC transplantation. Chimerism levels of mice injected with congenic HSPCs were checked 9 days postinfusion. Here, differences were observed; chimerism levels in the epiphysis and calvarium were higher than in diaphysis (Figure 5A-B), which was also associated with a higher frequency of donor cells with an LSK and LSK-CD150 phenotype (Figure 5C). After 3 weeks, the 3 BM compartments displayed homogeneous chimerism levels and similar frequencies of donor-derived HSPCs, appearing to have reestablished a neo–steady state (Figures 4 and 5B-C).

To understand the differences observed at day 9, we analyzed the homing efficiency after HSPC transplantation and found that LSK and LSK-CD150 do indeed home more efficiently in the calvarium and epiphysis as compared with diaphysis (Figure 5D). The apparent increase in homing efficiency to the calvarium might be explained, at least partly, by an increase in cell death in this BM compartment following irradiation (Figure 5E). However, this cannot explain the homing/reconstitution differences obtained between the epiphysis and diaphysis, because the radiosensitivity was lower in epiphysis.

From this, it appears that although BRA and BVF do not correlate with differences in steady-state niches, following irradiation and transplantation, hematopoietic reconstitution is faster in the sites displaying high BRA and BVF. This is likely due, at least in part, to more efficient HSPC seeding in these regions after intravenous administration.

Discussion

It has recently been reported that blood vessels and sinusoids can be found close to the bone.[14,15] Additionally, using histomorphometry and spatial distribution assays, Ellis et al[48] have reported similar observations in murine long bones, and very recently, Nombela-Arrieta et al[49] also found similar results in long bones using laser scanning cytometry. Here, the use of improved contrasting procedures allows us to quantify the extent of vascularization in all BM compartments. Taken together, it seems that sinusoids are, at the very least, structural components of the osteoblastic niche in flat and long bones. From this, it appears that former concepts based on the dichotomy of the osteoblastic and the vascular niches are not absolute. Rather, the osteoblastic niche, in close proximity to vasculature, is likely to also integrate some contributions from endothelial cells, pericytes, and/or mesenchymal stem cells and their respective secretomes.

In addition to the structural proximity of the vasculature to the endosteum, we have been able to quantitatively measure BVF and BRA and compare these features to other aspects of the niche. We
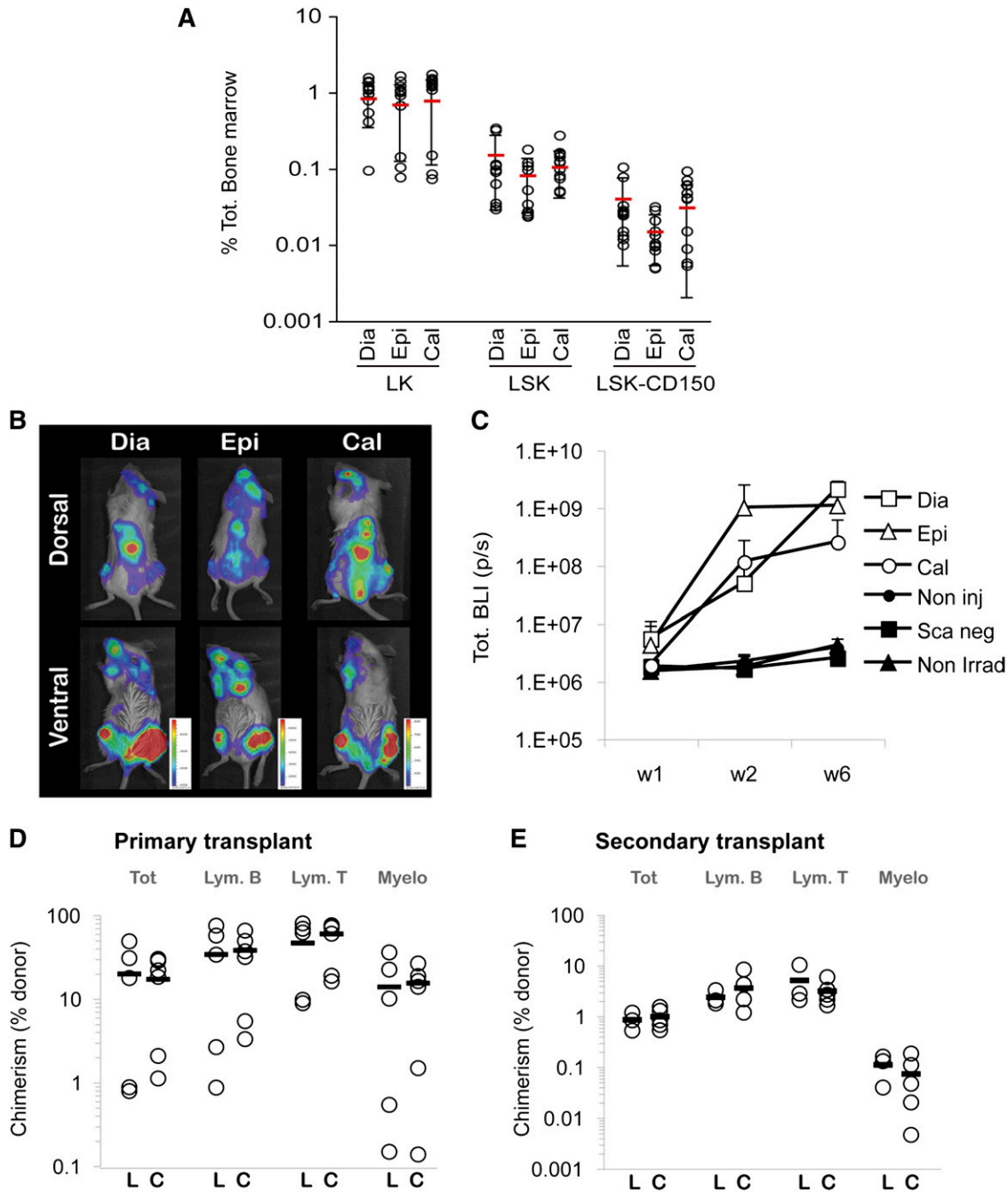
Figure 4. Qualitative and quantitative assessment of HSCs from different homeostatic BM compartments. (A) Percent of HSPC subpopulations from different BM compartments, $\pm$ SD, quantified by flow cytometry from wild-type animals (n = 14; C57Bl6 or β-actin-luciferase mice). (B) Noninvasive BLI tracking of 1250 LSK cells sorted from Dia, Epi, or Cal, 7 days postintravenous transplantation in sublethally irradiated NOD/SCID recipients. Signal localization is observed in BM compartments, such as the femur, tibia, vertebrae, and calvaria. (C) Noninvasive BLI quantification of hematopoietic reconstitution. Animals injected with 1250 LSK cells from the designated source (Dia, Epi, or Cal) were imaged after 1, 2, and 6 weeks postinjection. Data displayed are the average of BLI activity (photons per second) from 4 animals at week 1, 3 animals at week 2, and 2 animals at week 6, $\pm$ SD. No statistical difference was observed between these 3 groups. Negative controls included noninjected animals (Non Inj), sublethally irradiated NOD/SCID injected with lineage low Sca-1–negative sorted cells (Sca neg), or 1250 LSK from diaphysis injected in nonirradiated NOD/SCID recipients (Non irrad). (D) Chimerism of lethally irradiated CD45.2 primary recipients 13 weeks after being transplanted with 0.5×10^6 BM-leukocytes derived from the legs (L) or calvaria (C) of congenic (CD45.1) donors. Each circle represents the donor-derived chimerism level from each recipient (n = 5-6 per group) within the total leukocytes (CD45), B cells (B220), T cells (CD3), and myeloid cells (CD11b + CD11c). (E) Competitive secondary transplantation: percentage of chimerism of lethally irradiated CD45.2 recipients, 19 weeks after being transplanted with 10×10^6 unfractionated BM cells from the legs of primary recipients from (D) (n = 4-5 per group).

provide evidence that BVF, measured by in vivo fluorescence trapping, and perfusion efficiency are not always correlated. This indicates that BVF and distance from the blood vessel are not necessarily informative of the oxygenation of a specific region. Based on functional evidence, we confirm that LSK-CD150+ and LSK cells are less efficiently perfused than the more mature

populations, whatever the compartment analyzed. This confirms and extends previous reports.[11,12] However, we also observed that BM is much more efficiently perfused than the spleen, which is supposed to display very high perfusion efficiency. The detection of PIM in the different populations only partially correlates with these perfusion results as we found that the number of hypoxic
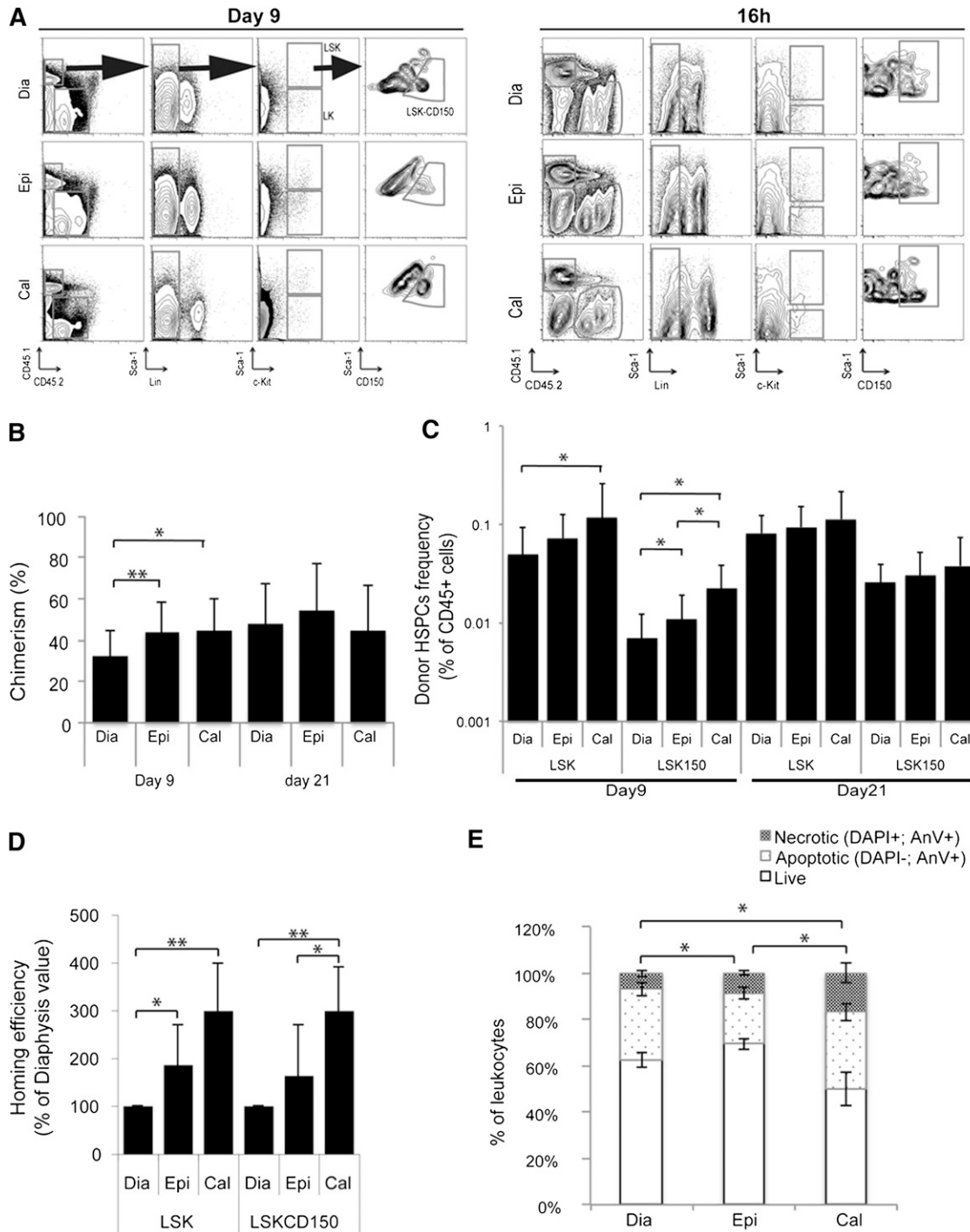
Figure 5. Macro-anatomical mapping of reconstituting stem cell niches. (A) Representative FACS plots showing the gating strategy used to analyze donor-derived chimerism 9 days (identical strategy used at day 21) posttransplantation (left). Gating strategy used to analyze HSPC homing efficiency at 16 hours (right panel). In order to ensure accuracy of the analysis at each time point, the precise positioning of the different gates was first performed on the recipient (CD45.2) HSPC subpopulations and then pasted on the donor cells (CD45.1). (B-C) Donor-derived chimerism 9 and 21 days postintravenous infusion of 2.3×10^5 to 10×10^5 lineage-depleted HSPCs (n = 10 and n = 8, respectively, 2 independent experiments). Total chimerism level (B) and frequency of donor-derived HSPCs as a frequency of total CD45+ BM cells (C). (D) Homing efficiency: 16 hours postintravenous infusion of 17×10^6 to 36×10^6 congenic CD45.1 BM-MNCs, diaphyses, epiphyses, and calvaria of the CD45.2 recipient were analyzed by flow cytometry (see A, right). The frequency of CD45.1+ LSK (LSK) and CD45.1+ LSKCD150 was calculated for 10^6 recipient (CD45.2+) cells and expressed as a percentage of the result obtained in the diaphysis in the same animal (n = 8, 2 independent experiments). (E) Analysis of cell viability 40 hours after lethal irradiation (time point where homing efficiency is being performed): BM cells were stained with 4',6-diamidino-2-phenylindole (DAPI) and Annexin V in order to quantify the frequency of live (DAPI$^-$ Annexin V$^-$), apoptotic (DAPI$^-$ Annexin V$^+$), and necrotic (DAPI$^+$ Annexin V$^+$) cells (n = 4).

cells and HSPCs is reduced in the calvarium as compared with the diaphysis. Interestingly, this corroborates the fact that BVF is higher in the calvarium as compared with diaphysis. In accordance with our finding, it has recently been reported that PIM reactivity in HSPCs is not necessarily a consequence of distance to the blood vessel but can also result from cell intrinsic features.[49] This raises questions with respect to the substantive nature of the hypoxic niche and whether it is a result of low oxygen levels or other niche-specific

microenvironmental factors that yet remain to be elucidated. We hope that technological developments, notably in the field of probes able to directly sense low oxygen levels in vivo, will permit an improvement in the localization of hypoxic niches in live BM and will also allow further investigation of this aspect of the niche.

As well as reporting new structural specificities of the calvarium, we have been able to demonstrate for the first time that this BM compartment is fully functional with respect the HSCs that reside there during homeostasis, homing, and reconstitution. Importantly, we show that the calvarium hosts HSC niches that are able to recruit and maintain primitive LT-HSCs and, in this respect, are indistinguishable from HSCs from the long bones. Because the calvarium develops through intramembranous ossification, this indicates that endochondral ossification is not necessary for the establishment and maintenance of functional HSC niches in adulthood, contrary to what has been reported for early development.[34]

Moreover, our study provides quantitative measurements allowing the direct comparison of BVF and BRA in different BM compartments from the same animal at steady state. Our results suggest that these biological parameters are macro-anatomical markers of reconstituting niches, but not steady-state HSC niches. Further studies will be needed to address the relevance and involvement of these markers in the homing, lodgment, and reconstitution process. Different studies have shown that irradiation-based conditioning induces blood vessel leakiness, which could potentially contribute to the homing process. Although we have looked at the impact of irradiation on BRA, we have not been able to detect any significant difference in this parameter (data not shown).

The marked difference observed in the localization of HSCs at steady state and shortly after transplantation (Figures 4 and 5B) is suggestive of 2 hypotheses: 2 distinct types of niches are being used during these different situations (reconstitution vs steady-state niches) or only a fraction of the steady-state HSC niches are being used during the reconstitution process due to differences in the trafficking of HSCs. In the latter situation, it is likely that the stem cell niches are not in the same physiological state at steady state and in the first days after irradiation. One of the major functions of the HSC niche at steady state is to maintain the quiescent status of HSCs. By contrast, recent data indicate that after irradiation, transplanted HSCs are actively cycling.[14,15] This raises the question of whether analyses of stem cell localization during the early phases of hematopoietic reconstitution are actually informative of the homeostatic, steady-state niche. Further studies will be needed to address this question, but our results highlight the fact that there might be differences between niche states, something that should be kept in mind when analyzing the literature.

A recent report by Nilsson's group shows a similar pattern of seeding in unconditioned recipients, reinforcing the notion that preferential seeding in the epiphysis over the diaphysis is independent of the long-term reconstitution potential (the calvarium was not studied in this report). The authors propose that increased expression of hyaluronan synthase 3 in the endothelial cells in these regions would favor a specific extravasation of HSPCs.[48] As HSPCs injected into an unconditioned environment, nonpermissive for long-term reconstitution (Figure 4C), are localized in similar macroscopic regions as compared with HSCs injected into conditioned recipients, questions are raised with respect to the definition of the reconstituting stem cell niche at early time points postinjection. Additionally, further questions are raised in consideration of engraftment dynamics and whether these stem cells are really lodged within their niche at this stage, or whether they are actually still navigating and on their way toward the niche. Further time-lapse intravital imaging should be able to address this question.

On a practical note, our data imply that monitoring chimerism levels in transplanted animals using BM sampling[50] should be used with caution, especially for early time points. Reliable quantitative information can be collected in a (neo)–steady state, but that might not be the case during the colonization process depending on the localization of the puncture (Figure 5A). This further illustrates the need for noninvasive whole body imaging approaches for long-term follow-up.

One of our specific aims in this study was to validate the calvarium as an appropriate model to study HSCs and their niches. Using a broad range of approaches, we can conclude that intravital imaging of the calvarium represents a powerful model to observe the dynamic behavior of BM cells within live, intact bones. To date, we are not aware of other imaging strategies able to achieve similar observations without inducing physical damage to the bone and/or the BM. Still, it should be kept in mind that each BM compartment displays unique properties that might, in specific conditions, have some as yet unknown effects on HSCs and/or their niches.

Altogether, we can conclude that despite structural heterogeneity in different BM compartments, homeostatic HSCs are evenly distributed throughout the skeleton in contrast with what is generally believed.[3,7,14,17] What drives the distribution of HSCs at steady state will need to be further elucidated. Although BVF and BRA do not correlate with steady-state HSC niches, these 2 parameters do appear to be markers of reconstituting niches. In this regard, the precise definition and understanding of the reconstituting niches to which HSCs home initially after transplantation remain to be determined.

Acknowledgments

Authorship

Contribution: F.L. led the conception and design of the experiments and collection, analysis, and interpretation of the data and wrote the manuscript; K.F., L.L.-O., and E.C. helped with realization of experiments and editing of the manuscript; and D.B. was responsible for conception and design, data analysis and interpretation, and redaction of the manuscript.

Conflict-of-interest disclosure: The authors declare no competing financial interests.

Correspondence: Dominique Bonnet, Haematopoietic Stem Cell Laboratory, London Research Institute, Cancer Research UK, 44 Lincoln's Inn Fields, WC2A3PX London, United Kingdom; e-mail: Dominique.Bonnet@cancer.org.uk; and Francois Lassailly, In Vivo Imaging, London Research Institute, Cancer Research UK, 44 Lincoln's Inn Fields, WC2A3PX London, United Kingdom; e-mail: francois.lassailly@cancer.org.uk.

References

1. Kiel MJ, Morrison SJ. Uncertainty in the niches that maintain haematopoietic stem cells. *Nat Rev Immunol.* 2008;8(4):290-301.

2. Papayannopoulou T, Scadden DT. Stem-cell ecology and stem cells in motion. *Blood.* 2008; 111(8):3923-3930.

3. Ehninger A, Trumpp A. The bone marrow stem cell niche grows up: mesenchymal stem cells and macrophages move in. *J Exp Med.* 2011;208(3): 421-428.

4. Fujisaki J, Wu J, Carlson AL, et al. In vivo imaging of Treg cells providing immune privilege to the haematopoietic stem-cell niche. *Nature.* 2011; 474(7350):216-219.

5. Yamazaki S, Ema H, Karlsson G, et al. Nonmyelinating Schwann cells maintain hematopoietic stem cell hibernation in the bone marrow niche. *Cell.* 2011;147(5):1146-1158.

6. Nilsson SK, Johnston HM, Coverdale JA. Spatial localization of transplanted hemopoietic stem cells: inferences for the localization of stem cell niches. *Blood.* 2001;97(8):2293-2299.

7. Zhang J, Niu C, Ye L, et al. Identification of the haematopoietic stem cell niche and control of the niche size. *Nature.* 2003;425(6960):836-841.

8. Avecilla ST, Hattori K, Heissig B, et al. Chemokine-mediated interaction of hematopoietic progenitors with the bone marrow vascular niche is required for thrombopoiesis. *Nat Med.* 2004; 10(1):64-71.

9. Tokoyoda K, Hauser AE, Nakayama T, Radbruch A. Organization of immunological memory by bone marrow stroma. *Nat Rev Immunol.* 2010; 10(3):193-200.

10. Trumpp A, Essers M, Wilson A. Awakening dormant haematopoietic stem cells. *Nat Rev Immunol.* 2010;10(3):201-209.

11. Parmar K, Mauch P, Vergilio JA, Sackstein R, Down JD. Distribution of hematopoietic stem cells in the bone marrow according to regional hypoxia. *Proc Natl Acad Sci USA.* 2007;104(13): 5431-5436.

12. Winkler IG, Barbier V, Wadley R, Zannettino AC, Williams S, Lévesque JP. Positioning of bone marrow hematopoietic and stromal cells relative to blood flow in vivo: serially reconstituting hematopoietic stem cells reside in distinct nonperfused niches. *Blood.* 2010;116(3):375-385.

13. Askenasy N, Stein J, Yaniv I, Farkas DL. The topologic and chronologic patterns of hematopoietic cell seeding in host femoral bone marrow after transplantation. *Biol Blood Marrow Transplant.* 2003;9(8):496-504.

14. Xie Y, Yin T, Wiegraebe W, et al. Detection of functional haematopoietic stem cell niche using real-time imaging. *Nature.* 2009;457(7225): 97-101.

15. Lo Celso C, Fleming HE, Wu JW, et al. Live-animal tracking of individual haematopoietic stem/progenitor cells in their niche. *Nature.* 2009; 457(7225):92-96.

16. Köhler A, Schmithorst V, Filippi MD, et al. Altered cellular dynamics and endosteal location of aged early hematopoietic progenitor cells revealed by time-lapse intravital imaging in long bones. *Blood.* 2009;114(2):290-298.

17. Lewandowski D, Barroca V, Ducongé F, et al. In vivo cellular imaging pinpoints the role of reactive oxygen species in the early steps of adult hematopoietic reconstitution. *Blood.* 2010;115(3): 443-452.

18. Mazo IB, Gutierrez-Ramos JC, Frenette PS, Hynes RO, Wagner DD, von Andrian UH. Hematopoietic progenitor cell rolling in bone marrow microvessels: parallel contributions by endothelial selectins and vascular cell adhesion molecule 1. *J Exp Med.* 1998;188(3):465-474.

19. Massberg S, Schaerli P, Knezevic-Maramica I, et al. Immunosurveillance by hematopoietic progenitor cells trafficking through blood, lymph, and peripheral tissues. *Cell.* 2007;131(5): 994-1008.

20. Adams GB, Alley IR, Chung UI, et al. Haematopoietic stem cells depend on Galpha(s)-mediated signalling to engraft bone marrow. *Nature.* 2009;459(7243):103-107.

21. Sipkins DA, Wei X, Wu JW, et al. In vivo imaging of specialized bone marrow endothelial microdomains for tumour engraftment. *Nature.* 2005;435(7044):969-973.

22. Lane SW, Wang YJ, Lo Celso C, et al. Differential niche and Wnt requirements during acute myeloid leukemia progression. *Blood.* 2011;118(10): 2849-2856.

23. Sanchez-Aguilera A, Lee YJ, Lo Celso C, et al. Guanine nucleotide exchange factor Vav1 regulates perivascular homing and bone marrow retention of hematopoietic stem and progenitor cells. *Proc Natl Acad Sci USA.* 2011;108(23): 9607-9612.

24. Junt T, Schulze H, Chen Z, et al. Dynamic visualization of thrombopoiesis within bone marrow. *Science.* 2007;317(5845):1767-1770.

25. Mazo IB, Honczarenko M, Leung H, et al. Bone marrow is a major reservoir and site of recruitment for central memory CD8+ T cells. *Immunity.* 2005;22(2):259-270.

26. Sapoznikov A, Pewzner-Jung Y, Kalchenko V, Krauthgamer R, Shachar I, Jung S. Perivascular clusters of dendritic cells provide critical survival signals to B cells in bone marrow niches. *Nat Immunol.* 2008;9(4):388-395.

27. Pereira JP, An J, Xu Y, Huang Y, Cyster JG. Cannabinoid receptor 2 mediates the retention of immature B cells in bone marrow sinusoids. *Nat Immunol.* 2009;10(4):403-411.

28. Naveiras O, Nardi V, Wenzel PL, Hauschka PV, Fahey F, Daley GQ. Bone-marrow adipocytes as negative regulators of the haematopoietic microenvironment. *Nature.* 2009;460(7252): 259-263.

29. van den Bos T, Speijer D, Bank RA, Brömme D, Everts V. Differences in matrix composition between calvaria and long bone in mice suggest differences in biomechanical properties and resorption: special emphasis on collagen. *Bone.* 2008;43(3):459-468.

30. Everts V, Korper W, Hoeben KA, et al. Osteoclastic bone degradation and the role of different cysteine proteinases and matrix metalloproteinases: differences between calvaria and long bone. *J Bone Miner Res.* 2006;21(9): 1399-1408.

31. Everts V, Korper W, Jansen DC, et al. Functional heterogeneity of osteoclasts: matrix metalloproteinases participate in osteoclastic resorption of calvarial bone but not in resorption of long bone. *FASEB J.* 1999;13(10):1219-1230.

32. Perez-Amodio S, Jansen DC, Schoenmaker T, et al. Calvarial osteoclasts express a higher level of tartrate-resistant acid phosphatase than long bone osteoclasts and activation does not depend on cathepsin K or L activity. *Calcif Tissue Int.* 2006;79(4):245-254.

33. Adams GB, Chabner KT, Alley IR, et al. Stem cell engraftment at the endosteal niche is specified by the calcium-sensing receptor. *Nature.* 2006; 439(7076):599-603.

34. Chan CK, Chen CC, Luppen CA, et al. Endochondral ossification is required for haematopoietic stem-cell niche formation. *Nature.* 2009;457(7228):490-494.

35. Colvin GA, Lambert JF, Abedi M, et al. Murine marrow cellularity and the concept of stem cell competition: geographic and quantitative determinants in stem cell biology. *Leukemia.* 2004;18(3):575-583.

36. Wang X, Rosol M, Ge S, et al. Dynamic tracking of human hematopoietic stem cell engraftment using in vivo bioluminescence imaging. *Blood.* 2003;102(10):3478-3482.

37. Cao YA, Wagers AJ, Beilhack A, et al. Shifting foci of hematopoiesis during reconstitution from single stem cells. *Proc Natl Acad Sci USA.* 2004; 101(1):221-226.

38. Lassailly F, Griessinger E, Bonnet D. "Microenvironmental contaminations" induced by fluorescent lipophilic dyes used for noninvasive in vitro and in vivo cell tracking. *Blood.* 2010; 115(26):5347-5354.

39. Gandillet A, Park S, Lassailly F, et al. Heterogeneous sensitivity of human acute myeloid leukemia to β-catenin down-modulation. *Leukemia.* 2011;25(5):770-780.

40. Zaheer A, Lenkinski RE, Mahmood A, Jones AG, Cantley LC, Frangioni JV. In vivo near-infrared fluorescence imaging of osteoblastic activity. *Nat Biotechnol.* 2001;19(12):1148-1154.

41. Simsek T, Kocabas F, Zheng J, et al. The distinct metabolic profile of hematopoietic stem cells reflects their location in a hypoxic niche. *Cell Stem Cell.* 2010;7(3):380-390.

42. Hale LP, Braun RD, Gwinn WM, Greer PK, Dewhirst MW. Hypoxia in the thymus: role of oxygen tension in thymocyte survival. *Am J Physiol Heart Circ Physiol.* 2002;282(4): H1467-H1477.

43. Calvi LM, Adams GB, Weibrecht KW, et al. Osteoblastic cells regulate the haematopoietic stem cell niche. *Nature.* 2003;425(6960):841-846.

44. Kiel MJ, Yilmaz OH, Iwashita T, Yilmaz OH, Terhorst C, Morrison SJ. SLAM family receptors distinguish hematopoietic stem and progenitor cells and reveal endothelial niches for stem cells. *Cell.* 2005;121(7):1109-1121.

45. Colmone A, Amorim M, Pontier AL, Wang S, Jablonski E, Sipkins DA. Leukemic cells create bone marrow niches that disrupt the behavior of normal hematopoietic progenitor cells. *Science.* 2008;322(5909):1861-1865.

46. Méndez-Ferrer S, Michurina TV, Ferraro F, et al. Mesenchymal and haematopoietic stem cells form a unique bone marrow niche. *Nature.* 2010; 466(7308):829-834.

47. Weissleder R. A clearer vision for in vivo imaging. *Nat Biotechnol.* 2001;19(4):316-317.

48. Ellis SL, Grassinger J, Jones A, et al. The relationship between bone, hemopoietic stem cells, and vasculature. *Blood.* 2011;118(6): 1516-1524.

49. Nombela-Arrieta C, Pivarnik G, Winkel B, et al. Quantitative imaging of haematopoietic stem and progenitor cell localization and hypoxic status in the bone marrow microenvironment. *Nat Cell Biol.* 2013;15(5):533-543.

50. Mazurier F, Gan OI, McKenzie JL, Doedens M, Dick JE. Lentivector-mediated clonal tracking reveals intrinsic heterogeneity in the human hematopoietic stem cell compartment and culture-induced stem cell impairment. *Blood.* 2004; 103(2):545-552.